AAS 10-179

A DYNAMICAL SYSTEMS APPROACH TO MICRO-SPACECRAFT AUTONOMY

Blair Brown[*] and Colin McInnes[†]

The drive toward reducing the size and mass of spacecraft has put new constraints on the computational resources available for control and decision making algorithms. The aim of this paper is to present alternative methods for decision making algorithms that can be introduced for micro-spacecraft. The motivation behind this work comes from dynamical systems theory. Systems of differential equations can be built to define behaviors which can be manipulated to define an action selection algorithm. These algorithms can be mathematically validated and shown to be computationally efficient, providing robust autonomous control with a modest computational overhead.

INTRODUCTION

Current research interest on spacecraft systems has a focus on miniaturisation. Concepts such as formation-flying and swarming[1,2] have demonstrated the advantages that can be gained from having a system comprised of a number of smaller spacecraft as opposed to one large platform. In doing so, and realising the benefits that are to be gained from such a change, introduces new issues that must be addressed. Such micro-spacecraft pose new challenges for on-board autonomy with limited computational overhead.

The idea for the new algorithms presented here is for the system to adapt itself to changes in its environment during its mission life. Using data from available sensors the algorithm will self-organize into what is the appropriate response that should be realised by the actuators. The actuator function can range from an upload or download of data to battery charging or Fault Detection Isolation and Recovery (FDIR).

Three different concepts for on-board autonomy will be investigated in this paper. Each of these concepts draws from ideas developed in dynamical systems theory[3,4]

The first of the three control algorithms uses hetero-clinic cycles[5,6] and bifurcation theory[7,8] A hetero-clinic cycle is a collection of solution trajectories that connect sequences of equilibria, periodic solutions or chaotic invariant sets via saddle-sink connections. Bifurcation theory captures changes in the qualitative or topological structure of a given family of differential equations. Combining these concepts permits a state-space to be generated that is representative of the autonomous system. As the system cycles, it moves between equilibria which represent particular actions of the autonomous system, such as battery charging, recording and transmitting data.

Secondly, an artificial potential function algorithm[9,10] is presented. Here each equilibria now represents a local minimum in the potential function. By associating a task to each minimum and

[*]Mechanical Engineering Department, University of Strathclyde, Glasgow G1 1XJ.
[†]Professor, Mechanical Engineering Department, University of Strathclyde, Glasgow G1 1XJ.

permitting the global potential to evolve as a function of the system parameters (battery charge and data stored), the solution to the system of differential equations implies an action selection.

The third control algorithm develops the idea of Lyapunov stability[11,12] through direct adaptive control (DAC). Such robust controllers desensitize the system to the uncertainties of the plant by varying the controller gains continuously. Here an attitude control DAC algorithm is presented that attempts to minimise the artificial potential of the system defined by state deficits. The state deficits define the state of the system with respect to the ideal state. As these deficits are inter-related the DAC algorithm must choose an appropriate attitude to bring the deficits closest to their minimum value.

Results from introducing each of the three controllers into a simple model of autonomous spacecraft in Earth orbit are presented. State-space mappings are presented along with an analysis of the action selection. The results from these models demonstrate that the use of modern dynamical systems theory to generate provable control algorithms appears to be a promising concept for computationally limited micro-spacecraft.

CONTROLLERS

Heteroclinic-Cycle Bifurcation Control

To demonstrate the use of concepts from dynamical systems theory, a simple model with a heteroclinic cycle action selection algorithm has been developed. The model involves a single satellite in orbit around the Earth with three states that in turn correspond to the action that the satellite may perform. Due to the fact the satellite has three states this corresponds to a three dimensional state space allowing easy visualization by keeping the dimensionality low. The orbital model is three dimensional although the satellite is in an equatorial low Earth orbit for simplicity. For the purposes of recording and transmitting there is one target and one ground station on the surface of the Earth for the respective action. The positions of the target and ground station are defined by some latitude and longitude angles α_T ϵ_T and α_{GS} ϵ_{GS} respectively with respect to the meridian on the rotating Earth. The orbit of the spacecraft is circular and at a height of 500km above the surface of the Earth, therefore $\epsilon_T = \epsilon_{GS} = 0$, with the Earth assumed to be a regular sphere.

The three dynamic states in the model are defined as 'deficits' of the three main actions that the satellite is capable of. These deficits, as discussed in previous work,[13] are defined in Eq.(1) - Eq.(3) as:

$$Battery\ Deficit\ d_b = \frac{batt_{max} - batt_{cur}}{batt_{max} - batt_{min}} \tag{1}$$

$$Information\ Deficit\ d_i = \frac{mem_{max} - mem_{cur}}{mem_{max}} \tag{2}$$

$$Transmit\ Deficit\ d_t = \frac{mem_{cur}}{mem_{max}} \tag{3}$$

where *batt* corresponds to the battery charge at current (*cur*), maximum (*max*) and minimum (*min*) values and *mem* corresponds to the data held in the satellite memory at current (*cur*) and maximum (*max*) values. The magnitude of d_b increases as energy in the battery is consumed. The

magnitudes of d_i and d_t hold an inverse relationship. By recording data d_t increases while d_i decreases, while downlinking data causes d_i to increase while d_t decreases.

Models of subsystems that describe battery charging/dis-charging and the telemetry needed to record and transmit data from relevant ground station and target locations are included in the simulation model. Therefore, the states of the system are linked, with the battery discharging as data is recorded and downlinked.

The new concept presented here is the action-selection algorithm and is built around the Guckenheimer-Holmes (GH) heteroclinic cycle.[14] This is an example of a heteroclinic cycle involving three equilibrium solutions of a system of ordinary differential equations (ODE) proposed by Guckenheimer and Holmes, Eq.(4)-(6), with state variables (*x,y,z*):

$$\dot{x} = x - (Ax^2 + By^2 + Cz^2)x + \epsilon y \tag{4}$$

$$\dot{y} = y - (Cx^2 + Ay^2 + Bz^2)y + \epsilon z \tag{5}$$

$$\dot{z} = z - (Bx^2 + Cy^2 + Az^2)z + \epsilon x \tag{6}$$

Depending on the initial conditions set, cycling behavior results between three equilibrium positions. It is these three equilibrium positions that will constitute the three actions of the algorithm. To generate the action selection algorithm a new form of the above equation set, Revised Guckenheimer-Holmes (RGH), is proposed that permits different behavior. The RGH equation set is shown in Eq.(7)-(9):

$$\dot{x} = \Omega x - (A_1x^2 + By^2 + Cz^2)x + \epsilon y \tag{7}$$

$$\dot{y} = \Omega y - (Cx^2 + A_2y^2 + Bz^2)y + \epsilon z \tag{8}$$

$$\dot{z} = \Omega z - (Bx^2 + Cy^2 + A_3z^2)z + \epsilon x \tag{9}$$

A schematic describing the three dimensional state-space is shown in Fig.(1). Each axis of the state-space corresponds to one state variable in the above equation set. The dots denote the positions of the equilibrium point that correspond to the respective action.

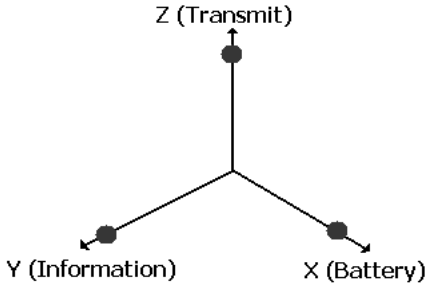

Figure 1. Three dimensional state-space with associated actions: x(charge battery), y(record data), z(downlink data)

The RGH equations permit the ODEs to stop cycling by introducing three individual parameters A_i that correspond to the three state deficits. Also included in these control parameters is the degree of 'availability', where the control deficit is weighted by a function of the cosine of the angle between the satellite and target/ground station location, i.e. a function which represents the visibility of the target or ground station. Whenever one of these parameters becomes dominant the corresponding attractor does not permit the cycling to continue and an action is determined according to the location in state space. Similarly, the availability of battery charging is unity in sunlight and zero in eclipse. The inclusion of the parameter Ω increases the frequency of the cycle so there is less time lag between changes in action selection.

This type of controller has advantages. No set sequence of events must occur before an action is selected like in the case of neural networks. Some similarities can be drawn between this controller and a neural network however, the idea of a threshold being broken for an action to prevail is comparable to the threshold signals between neurons that induce an output. Aspects of neural network design could therefore be used to improve on the efficiency of the heteroclinic controller. Also the stability of the set of differential equation can be proven by analysis.

Spacecraft Model

In order to demonstrate the practicality of the method described, results from the model are presented. The first of these is the state space mappings. A comparison can be drawn between the GH equation set and the RGH equation set from Fig.(2) and (3) respectively. In Fig.(2) the GH cycle, starting form some arbitrary point, is evident in a continual cycle moving between the three equilibrium positions. Alternatively, in the RGH equation set, with one control parameter set to dominate, Fig.(3) depicts the cycle being broken and the state space coming to rest at a particular equilibrium position.

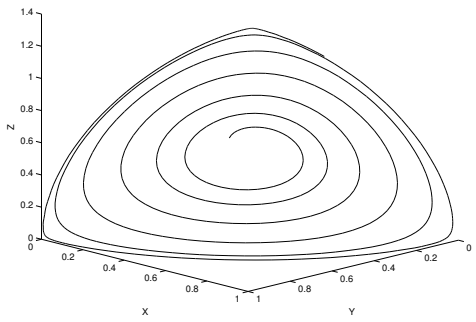

Figure 2. Demonstration of GH cycle

Secondly an analysis of the action selection output is provided. In this case the same model is setup to run for one Earth day. This permits the satellite to pass over both the target and the ground station several times and also pass in and out of the Earth's shadow with battery charge and discharge. Over the one day simulation the satellite's deficits vary along with the availabilities, leading to a control parameter or 'potential' becoming dominant. When the magnitude of this potential passes a certain threshold the model selects the appropriate action. This process can be seen in Fig.(4) and (5), where the different peaks in Fig.(4) correspond to the different action integers seen in Fig.(5). The first integer represents the charge action, the second integer the record action

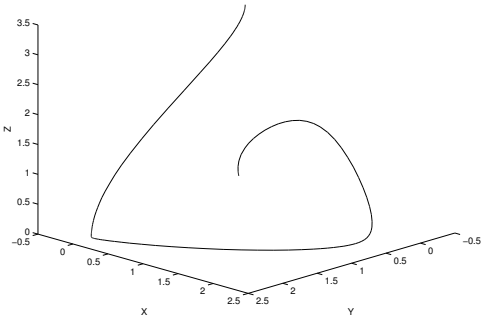

Figure 3. Demonstration of RGH cycle

and the third integer represents the transmit action. The fourth integer denotes a state of 'drift' where none of the three actions may be realised. Fig.(6) depicts the data in the satellite memory as the simulation progresses and Fig.(7) depicts the corresponding charge of the battery.

The orbital scenario was chosen for simplicity and to allow the different prerequisites for each action to occur during each orbit. This can be seen in Fig.(5) when the control algorithm selects an approximate sequence of record-transmit-charge, with drift periods in between, during each orbit. This comes as a consequence of each of the respective bifurcations taking place and leading to an appropriate potential, corresponding to the respective action, becoming dominant, as is seen in Fig.(4). The efficiency of the algorithm is detailed in the memory and battery charge of the satellite, given in Fig.(6 - 7), the volume of memory present in the memory over a cycle is approximately five percent from being at full and empty capacity implying the control algorithm is making full use of most of the memory available, and similarly there is a large discharge depth in the battery.

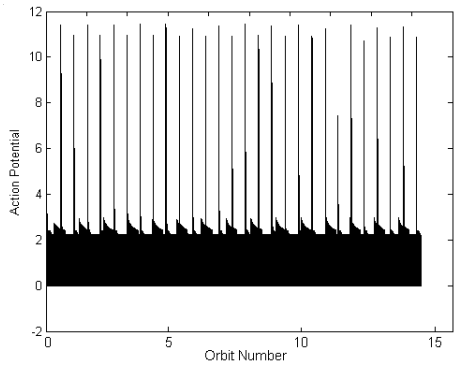

Figure 4. Model output for action potentials

Artificial Potential Field Control

The second control algorithm presented adopts the ideas of the artificial potential field[15].[16] An artificial potential field can be defined by a system of ordinary differential equations (ODEs) that incorporate state parameters similar or equal to those used in the heteroclinic control method. Solving the system of ODEs, and by manipulation of this predetermined field, can then lead to a range of different control actions being selected.

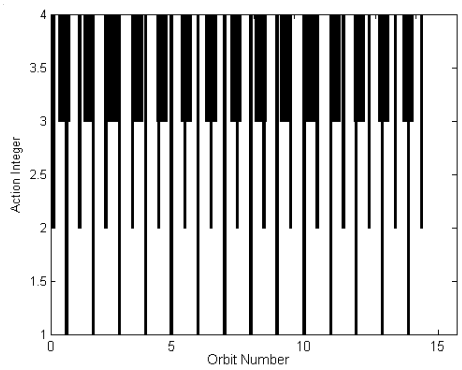

Figure 5. Model output for action selection

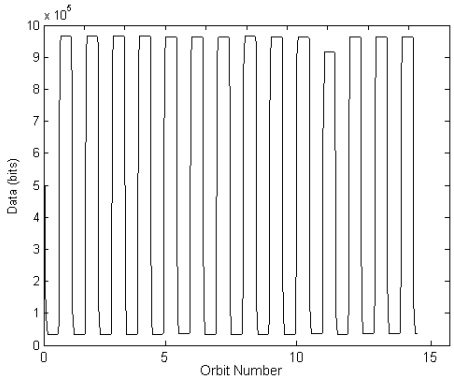

Figure 6. Model output for data in satellite memory

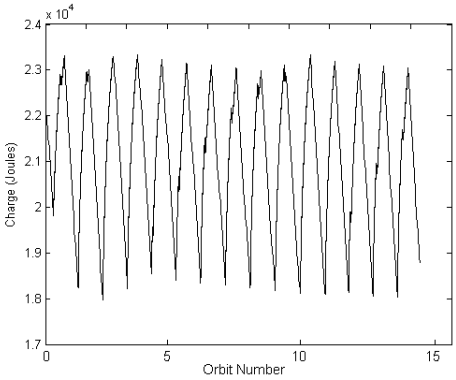

Figure 7. Model output for satellite battery charge

Each action in this algorithm is defined by a potential local minimum. This local minimum can be defined to be in any location of the potential field and be a function of a state deficit.

First, consider one local minimum given by an artificial potential *V*, defined by Eq.(10).

$$V = d_i.e^{-\lambda_i.((X-\rho_x)^2+(Y-\rho_y)^2)} \tag{10}$$

where d_i is the state deficit, λ controls the diameter of the minima, *X* and *Y* are the range of artificial potential field in the x and y axis respectively and [ρ_x,ρ_y] defines the position of the local minima on the artificial field. A plot of such a field and minima is shown in Fig.(8), where $d_i = 1$, $\lambda = 1$, $-2 \leq X \leq 2$, $-2 \leq Y \leq 2$ and [ρ_x,ρ_y] = [0,0].

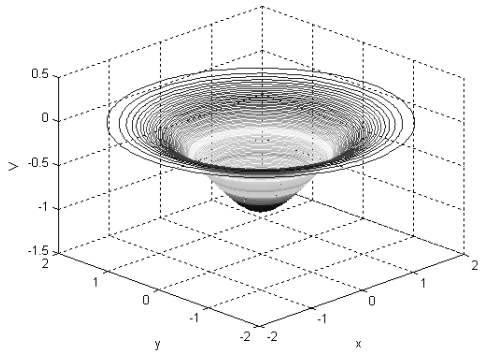

Figure 8. Single potential minimum

If the negative derivative of the potential is calculated with respect to each axis of the potential field then the solution to this set of partial differential equations tends to [ρ_x,ρ_y] due to the overlap in the radius of the local minimums included in the placement process, i.e:

$$\dot{x} = -\frac{\partial V}{\partial x} \tag{11}$$

$$\dot{y} = -\frac{\partial V}{\partial y} \tag{12}$$

The process of adding multiple minima to a potential field permits the creation of a set of differential equations that can be a function of the system (satellite) deficits and physical parameters. This potential field can then be used to develop action selection control algorithms.

Single Spacecraft Model For the single spacecraft model the same control actions as for the heteroclinic model are selected, i.e. charge battery, record, transmit and drift. This pertains to four different local minima that are located on the potential field. If one action is more important than another then it has a more central geometric location and the solver more frequently tends to this location. For this model each of the three main tasks (charge, record, transmit) are of assumed equal importance and are equally spaced around a circle of radius 1 centered at [0,0]. The ρ_C, ρ_R and ρ_T coordinates that correspond to the local minima location for charge, record and transmit respectively are therefore:

$$[\rho_C^x, \rho_C^y] = [1, 0]$$

$$[\rho_R^x, \rho_R^y] = [-0.5, cos(\frac{\pi}{6})]$$

$$[\rho_T^x, \rho_T^y] = [-0.5, -cos(\frac{\pi}{6})]$$

$$[\rho_D^x, \rho_D^y] = [0, 0]$$

where, ρ_D is the fourth drift state that the system can choose.

With reference to Eq.(10) the three state deficits that correspond to the three main actions d_b, d_i and d_t (charge, record, transmit respectively) are defined by equations 1 - 3. The values of λ_i determine the radius of the local minima and in doing so also the gradient of the slope of each minima. To equalise the system the three parameters are set to $\lambda_b = \lambda_i = \lambda_t = 1$, again corresponding to charge, record, and transmit respectively.

Finally, values for the drift minimum are selected. The drift action will only be selected if none of the other three actions are available. To this end the drift minimum must act as an all encompassing safety-net. Here the deficit value is set to $d_d = 0.1$ so it does not influence the selection of any other action when they are available. Also, the drift minimum must cover the entire area of the potential field and to this end the value of λ_d is set to $\lambda_d = 0.5$, which defines it to be much wider than the other minima with a shallower gradient.

The final potential field is therefore defined by:

$$\begin{aligned} V = & d_b.e^{-\lambda_b.((X-\rho_C^x)^2+(Y-\rho_C^y)^2)} \\ & +d_i.e^{-\lambda_i.((X-\rho_R^x)^2+(Y-\rho_R^y)^2)} \\ & +d_t.e^{-\lambda_t.((X-\rho_T^x)^2+(Y-\rho_T^y)^2)} \\ & +d_d.e^{-\lambda_d.((X-\rho_D^x)^2+(Y-\rho_D^y)^2)} \end{aligned} \tag{13}$$

Examples of the potential field are given in Fig.(9). In Fig.(9)(a) the deficit values are $d_b = 0.9$, $d_i = 0.5$, $d_t = 0.1$, $d_d = 0.1$ and it can be seen that the differential equation solver will tend to the location of the local minimum for the charge action at [0,1]. In Fig.9(b) the deficit values are neglected as neither the sun, record target, or transmit target can be seen, therefore the only minimum on the potential field is the drift action and the differential equation solver tends to [0,0], the location of the drift minimum.

Results for the incorporation of the control algorithm into the orbital model are shown in Fig.(10) - (13). The orbital parameters for this simulation are the same as those chosen for the heteroclinic simulation, i.e. a spacecraft in a circular orbit 500km above the surface of the Earth, with the ground station and target placed at desired longitudes and latitudes. Fig.(10) shows a plot of the

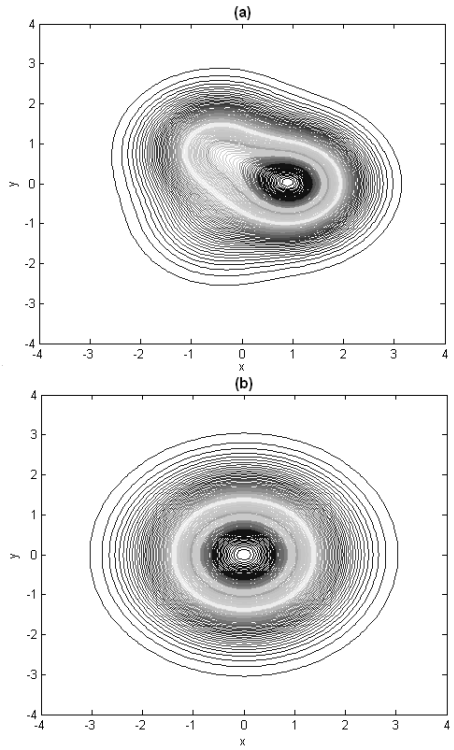

Figure 9. Multiple minimum in the potential field

phase plane during simulation. The plot shows the solver moving from the central drift state to the appropriate action locations whenever they become available. Fig.(11) depicts the action selection process, as the satellite moves in and out of eclipse or has access to the record and transmit targets the appropriate action can be seen to be selected. The first integer represents the charge action, the second the record action, the third represents the transmit action and the fourth denotes the drift state.

The battery charge and data stored are shown in Fig.(12) and Fig.(13) respectively. The battery can be seen to cycle through a charge-discharge state and the record and transmit actions can be seen as the satellite memory is filled and emptied.

This scenario does not put demand on the algorithm. In addition, the output of the algorithm essentially maps the deficit directly to specific actions. However, for more complex problems the use of the potential field allows a mediation between multiple competing behaviors. In the following section a fourth option will be given to the satellite where it may transfer data to another satellite in the same orbit but further ahead or behind the specific satellite under investigation in order to off-load data and so load-balance across multiple satellites.

Multi-Spacecraft Model One of the main interests in micro-spacecraft is the benefit that can be gained in flying a constellation of satellites[17].[18] A similar control algorithm to that proposed in the previous section will be implemented where the satellite has the option to transfer to an identical adjacent satellite.

The local minimum for the potential field is constructed using Eq.(10). Here there are five actions

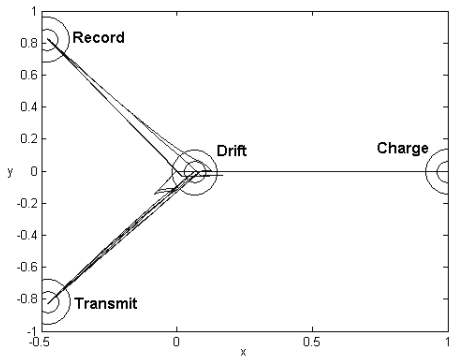

Figure 10. PF phase plane

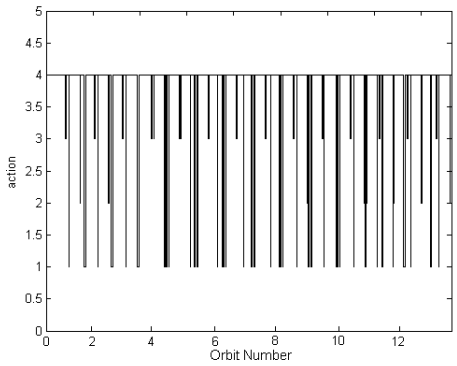

Figure 11. PF actions

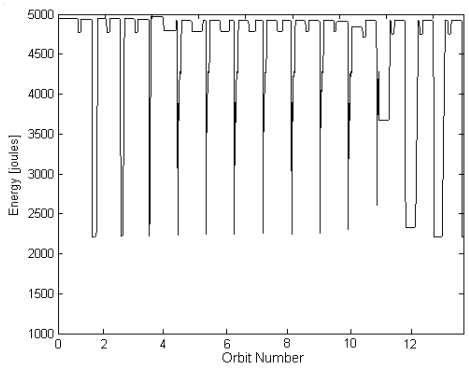

Figure 12. PF battery

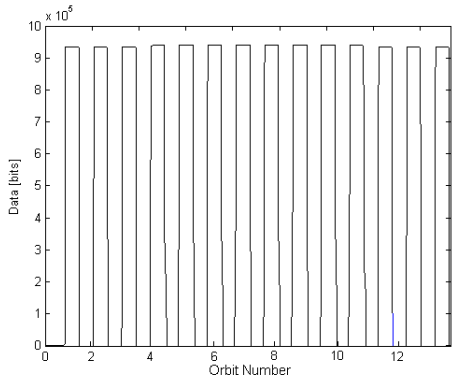

Figure 13. PF memory

that can be selected: charge, record, transmit to ground station, transmit to a neighboring satellite, and drift. The location of the minima are as follows:

$$[\rho_C^x, \rho_C^y] = [1, 0]$$

$$[\rho_R^x, \rho_R^y] = [0.309, -0.951]$$

$$[\rho_T^x, \rho_T^y] = [0.309, 0.951]$$

$$[\rho_D^x, \rho_D^y] = [0, 0]$$

$$[\rho_{IF}^x, \rho_{IF}^y] = [-0.809, 0.588]$$

$$[\rho_{IB}^x, \rho_{IB}^y] = [-0.809, -0.588]$$

where ρ_{IF} ρ_{IB} are the inter-satellite links for the satellite forward and back respectively. Both satellites can always be seen by the primary satellite, this is guaranteed by selection of a orbital hight of above 450km. The deficit for the inter-satellite link for the forward satellite is defined as:

$$d_{sf} = 2.mem_{pri}/(mem_{max} + mem_{pri} + mem_{sec}) \tag{14}$$

where mem_{pri} is the data in the memory of the primary satellite, mem_{sec} is the data in the memory of the secondary satellite and mem_{max} is the maximum data the satellite can hold. A similar relation is built for the other satellite. The potential field is now defined as:

$$\begin{aligned} V = {} & d_b.e^{-\lambda_b.((X-\rho_C^x)^2+(Y-\rho_C^y)^2)} + d_i.e^{-\lambda_i.((X-\rho_R^x)^2+(Y-\rho_R^y)^2)} \\ & + d_t.e^{-\lambda_t.((X-\rho_T^x)^2+(Y-\rho_T^y)^2)} + d_d.e^{-\lambda_d.((X-\rho_D^x)^2+(Y-\rho_D^y)^2)} \\ & + d_{sf}.e^{-\lambda_{sf}.((X-\rho_{IF}^x)^2+(Y-\rho_{IF}^y)^2)} + d_{sb}.e^{-\lambda_{sb}.((X-\rho_{IB}^x)^2+(Y-\rho_{IB}^y)^2)} \end{aligned} \tag{15}$$

An example of this potential field is given in Fig.(14). Here the state deficits are: $d_b = 0.1$, $d_i = 0.1$, $d_t = 0.9$, $d_d = 0.1$, $d_{sf} = 0.5$, and $d_{sb} = 0.5$. In this case the satellite now has two local minimum present and the action selected will depend on the position on the potential field and the local gradients. In this example the deficit corresponding to the transmission action is larger than the deficits corresponding to the inter-satellite links so the probability that the satellite will choose to transmit to the ground is more likely but this also depends on the previous action selected, i.e. corresponding to the prior location on the potential field.

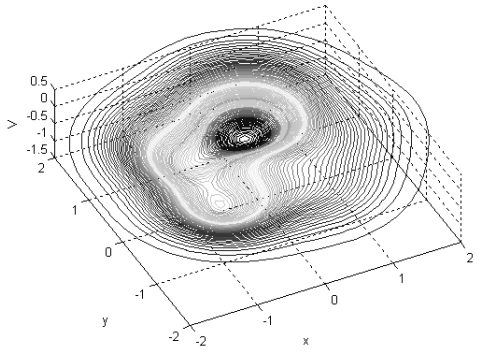

Figure 14. PF multi-spacecraft potential field

Results for the inclusion of the enhanced control law into the orbital model are shown in Fig.(15) - (18). Fig.(15) shows the phase-plane for the controller during the simulation period. The associated actions are given in Fig.(16), where the integers 1, 2, 3, 4, 5, and 6 correspond to charge, transmit, record, forward inter-satellite link, backward inter-satellite link, and drift respectively. Battery charge and discharge can be seen in Fig.(17), and the data stored in each satellite is shown in Fig.(18).

DAC

Robust controllers try to desensitise a control system to the uncertainties of the plant. An adaptive controller aims to allow controller gains to vary continuously allowing for uncertainty and therefore increasing system performance during control implementation.

In,[19] it was demonstrated that direct adaptive controllers can be applied to nonlinear oscillators. In,[20] the concept was further proven in the use of electromagnetically controller oscillators and pneumatic cylinders. The concept has also been applied to other problems[21].[22]

Here, a direct adaptive control law is presented that provides robust action selection for a micro-spacecraft. It is shown that the control law is a function of known system parameters while being

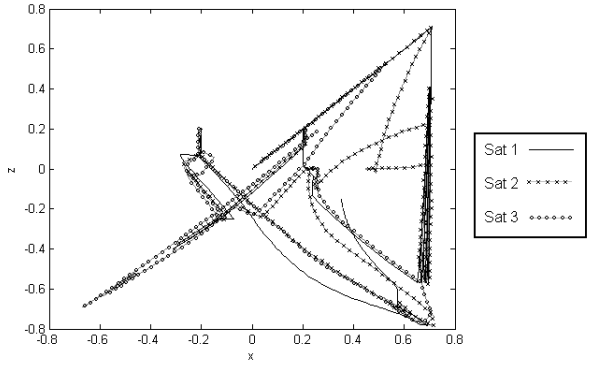

Figure 15. PF multi-spacecraft phase plane

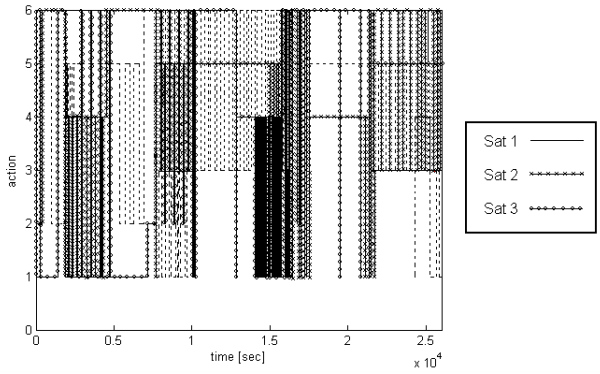

Figure 16. PF multi-spacecraft actions

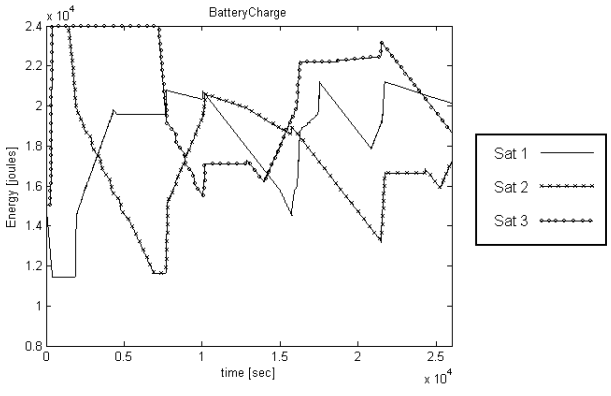

Figure 17. PF multi-spacecraft battery

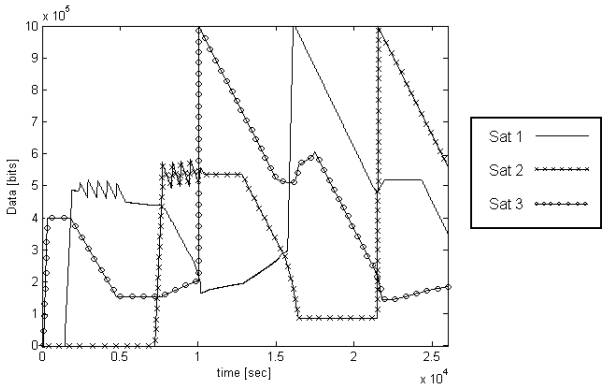

Figure 18. PF multi-spacecraft memory

independent of external disturbances. DAC is therefore demonstrated as an attractive option for the micro-spacecraft problem since fault detection isolation and recovery (FDIR) is embedded into the system.

State Feedback for Micro-Spacecraft Model The theorem for adaptive control is defined in associated literature[19] and can be applied to the micro-spacecraft action selection problem. As the control law, by definition, is applicable to linear systems, all the non-linearities associated with the orbital model make the orbital model in the previous two sections inappropriate. With this in mind a different model is created for application of the DAC controller.

It will be assumed that the control is the spacecraft pointing direction and that the spacecraft slews between three different directions corresponding to the required action (Sun pointing for battery charging etc).

To implement the control law the system state differential equations, in this case the spacecraft deficits, defined by Eqs.(1 -3) must be a function of the controlled variable, in this case the spacecraft pointing angle ξ, with the aim of driving all deficits to zero. To build a model capable of being controlled in this manner a linear relationship for the variation of each of these deficits is created. A visualisation of the model is shown in Fig.(19)(b) and the linear differential equations governing the deficit relations are given by Eq.(16) and Eq.(17), for the battery deficit. The equations for the information deficit and transmission deficit are the same although centered on a different angular position as indicated in Fig.(19), and given by Eqs.(19 - 21). Note that the relationship between the information deficit (record) and transmission deficit (transmit) implies a selection of one action incurs a change in both deficits.

In Fig.(19)(a) the locations of the maximum charge, record, and transmit actions are ξ_{cha}, ξ_{rec} and ξ_{tra}. The lines depicting the triangular regions running off from each of these three points define the linear change in the magnitude of each of the three actions that decrease from a maximum when pointing directly at either of the three action until zero when at 30 degrees ($\xi_{\frac{1}{2}band}$) in a positive or negative sense from any of the maximum locations.

The model is defined as:

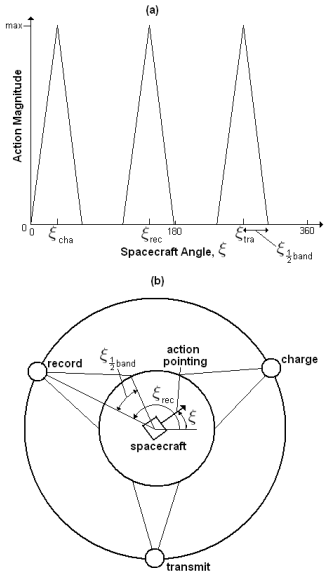

Figure 19. DAC action selection model

$$\begin{aligned}\dot{d}_b = \;& \dot{e}_{max}.(1 + ((\xi/(\xi_{cha} - Nb_{pos}.\xi_{\frac{1}{2}band})) \\ & -(\xi_{cha}/(\xi_{cha} - Nb_{pos}.\xi_{\frac{1}{2}band})))) \\ & for \quad (\xi - \xi_{\frac{1}{2}band}) \leq \xi \leq \xi_{cha}\end{aligned} \tag{16}$$

$$\begin{aligned}\dot{d}_b = \;& 3.\dot{e}_{max}.(1 - ((\xi/(\xi_{cha} + Nb_{neg}.\xi_{\frac{1}{2}band})) \\ & +(\xi_{cha}/(\xi_{cha} + Nb_{neg}.\xi_{\frac{1}{2}band})))) \\ & for \quad \xi_{cha} < \xi \leq (\xi + \xi_{\frac{1}{2}band})\end{aligned} \tag{17}$$

$$\begin{aligned}\dot{d}_i = \;& \dot{r}_{max}.(1 + ((\xi/(\xi_{rec} - Ni_{pos}.\xi_{\frac{1}{2}band})) \\ & -(\xi_{rec}/(\xi_{rec} - Ni_{pos}.\xi_{\frac{1}{2}band})))) \\ \dot{d}_t = \;& \dot{t}_{max}.(-1 - ((\xi/(\xi_{rec} - Ni_{pos}.\xi_{\frac{1}{2}band})) \\ & -(\xi_{rec}/(\xi_{rec} - Ni_{pos}.\xi_{\frac{1}{2}band})))) \\ \dot{d}_b = \;& \dot{e}_{cha}.(\dot{e}_{max}/(batt_{max} - batt_{min})) \\ & for \quad (\xi - \xi_{\frac{1}{2}band}) \leq \xi \leq \xi_{rec}\end{aligned} \tag{18}$$

$$\begin{aligned}\dot{d}_i = \;& 11.\dot{r}_{max}.(1 - ((\xi/(\xi_{rec} + Ni_{neg}.\xi_{\frac{1}{2}band})) \\ & +(\xi_{rec}/(\xi_{rec} + Ni_{neg}.\xi_{\frac{1}{2}band})))) \\ \dot{d}_t = \;& 11.\dot{t}_{max}.(-1 + ((\xi/(\xi_{rec} + Ni_{neg}.\xi_{\frac{1}{2}band})) \\ & +(\xi_{rec}/(\xi_{rec} + Ni_{neg}.\xi_{\frac{1}{2}band})))) \\ \dot{d}_b = \;& \dot{e}_{cha}.(\dot{e}_{max}/(batt_{max} - batt_{min})) \\ & for \quad \xi_{rec} < \xi \leq (\xi + \xi_{\frac{1}{2}band})\end{aligned} \tag{19}$$

$$
\begin{aligned}
\dot{d}_t = \;& \dot{t}_{max}.(1 + ((\xi/(\xi_{tra} - Nt_{pos}.\xi_{\frac{1}{2}band})) \\
& -(\theta_{tra}/(\xi_{tra} - Nt_{pos}.\theta_{\frac{1}{2}band})))) \\
\dot{d}_i = \;& \dot{r}_{max}.(-1 - ((\xi/(\xi_{tra} - Nt_{pos}.\xi_{\frac{1}{2}band})) \\
& -(\xi_{tra}/(\xi_{tra} - Nt_{pos}.\xi_{\frac{1}{2}band})))) \\
\dot{d}_b = \;& \dot{e}_{tra}.(\dot{e}_{max}/(batt_{max} - batt_{min})) \\
& for \quad (\xi - \xi_{\frac{1}{2}band}) \leq \xi \leq \xi_{tra}
\end{aligned}
\tag{20}
$$

$$
\begin{aligned}
\dot{d}_t = \;& 19.\dot{t}_{max}.(1 - ((\xi/(\xi_{tra} + Nt_{neg}.\xi_{\frac{1}{2}band})) \\
& +(\xi_{tra}/(\xi_{tra} + Nt_{neg}.\xi_{\frac{1}{2}band})))) \\
\dot{d}_i = \;& 19.\dot{r}_{max}.(-1 + ((\xi/(\xi_{tra} + Nt_{neg}.\xi_{\frac{1}{2}band})) \\
& +(\xi_{tra}/(\xi_{tra} + Nt_{neg}.\xi_{\frac{1}{2}band})))) \\
\dot{d}_b = \;& \dot{e}_{tra}.(\dot{e}_{max}/(batt_{max} - batt_{min})) \\
& for \quad \xi_{tra} < \xi \leq (\xi + \xi_{\frac{1}{2}band})
\end{aligned}
\tag{21}
$$

where $\dot{e}_{max}$ is the maximum charge rate, $\dot{r}_{max}$ is the maximum record rate and $\dot{t}_{max}$ is the maximum transmission rate. ξ_{cha} is the angular position of the maximum charge rate, 30 degrees, ξ_{rec} is the angular position of the maximum record rate, 150 degrees, and ξ_{tra} is the angular position of the maximum transmission rate, 270 degrees. $\xi_{\frac{1}{2}band}$ is half the angular width of the band within which each action occurs, 30 degrees. Nb_{pos}, Nb_{neg}, Ni_{pos}, Ni_{neg}, Nt_{pos} and Nt_{neg} are positive integers that define the slope of the linear dependance of each of the associated action rates - they are 0, 2, 4, 6, 8, and 10 respectively. Altogether Eqs.(16 - 21) defined the linear model from which an angle will associate a given action selected by the control algorithm.

When the system is in any of the other regions between the action selection regions white noise is included in the system through the ϕ control parameter. This stops the system for settling into one of these positions.

The control objective is to bring each of the systems deficits to zero. Defining the state $\mathbf{x} = [d_b\ d_i\ d_t]^T$, the control $u(t) = \xi$, and bringing together Eqs.(16 - 21), we obtain a set of linear differential equations:

$$
\dot{\mathbf{x}}(t) = \mathbf{A}.\mathbf{x}(t) + \mathbf{B}.u(t) + \mathbf{d} \tag{22}
$$

where $\mathbf{A}$ is zero and the other vectors are a function of ξ, and $\mathbf{B}$ and $\mathbf{d}$ are constructed from the relevant components from Eqs.(16 - 21).

From section 2.6.1, solving Lyapunov's equation using the general solutions to *R* and *P* maintaining A_s asymmetrically stable gives the variable control gains to the problem as:

$$
\dot{K_1}(t) = -(0.1d_b^2 + 0.01d_bd_i - 0.01d_bd_t) \tag{23}
$$

$$
\dot{K_2}(t) = -(0.001d_t^2 - 0.001d_bd_i - 0.001d_id_t) \tag{24}
$$

$$\dot{K_3}(t) = -(0.001d_t^2 - 0.001d_b d_t - 0.001d_i d_t) \tag{25}$$

$$\dot{\phi}(t) = -(0.01d_b^2 - 0.015d_i^2 + 0.015d_t^2) \tag{26}$$

This in turn leads to the control:

$$u(t) = K_1 d_b + K_2 d_i + K_3 d_t + \phi \tag{27}$$

The advantage of using this control algorithm is due to the fact it can react in real time to any disturbance, in this case d.

The results from the simulations of the DAC action selection controller are given in Figs.(20 - 22). Fig.(20) depicts the deficits of the satellite changing as different actions are selected. Fig.(21) shows the corresponding values of ξ that lead to the action selection. Fig.(22) shows the real time changing gains that define the control angle choice.

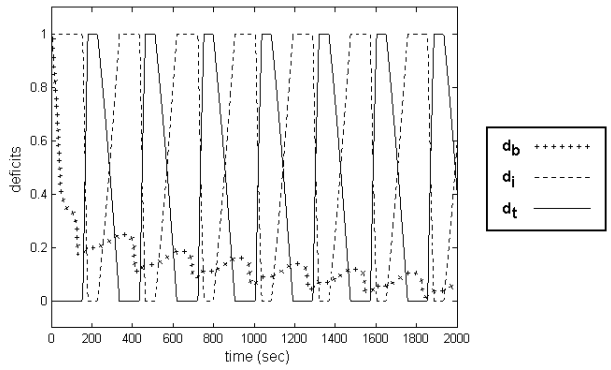

Figure 20. Action deficits

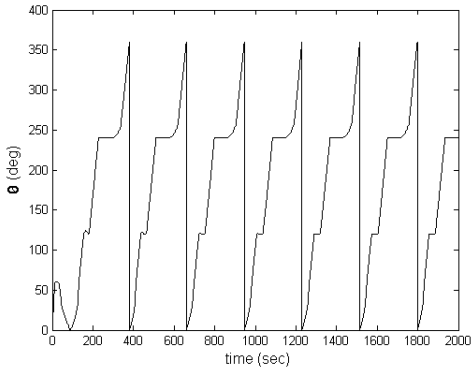

Figure 21. Control angle selection

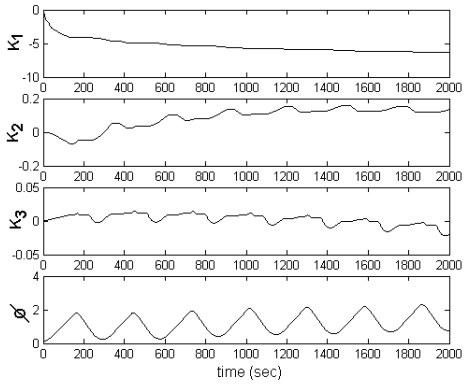

Figure 22. DAC gains

CONTROLLER COMPARISON

It has been demonstrated in this paper that dynamical systems theory can be used in a variety of different ways to enable micro-spacecraft autonomy. However, each of these controllers have differing merits and are suitable to a range of applications. For a simple (terrestrial or space-based) robotic application, the potential field controller is more applicable because the algorithm can be optimised to a specific task where little or no FDIR will be required as the environment that the controller works in has little uncertainty.

The potential field controller does begin to degrade in performance when a greater number of control actions are required due to the physical locations of the individual local minimums interfering with one another. this is because of the possibility of two attractors of equal potential occurring simultaneously. In this case, where a larger number of controllable actions are required then a controller resembling the heteroclinic-cycle bifurcation controller is more desirable. Although the heteroclinic-cycle controller similarly defines physical bifurcation locations for each of the actions, the heteroclinic cycle is a separate attractor altogether until a bifurcation threshold is passed and therefore there is no limit as to how many actions can be added to the controller. This controller requires slightly more processing computation that the potential field method.

The DAC control brings together the best of both the two other methods. Due to the control action being a direct result of realtime changes in the control gains, that in turn vary in real-time with the internal system states and external environmental, this controller is capable of dealing with significant uncertainty. This makes the DAC method ideal for controlling any system where there is little or no information about the environment where the system is to be operated.

CONCLUSIONS

This paper demonstrates the use of dynamical system theory as applied to micro-spacecraft autonomy. Three algorithms are defined and applied to the problem and the relative merits of each are assessed and compared. The outcome of this study suggests that a controller should be chosen on the merits of how much is known about the plant and the environment in which the system is to operate. More well known environments with few action options can utilize more simple potential field controllers, a greater number of control options merits a more complex heteroclinic-cycle bifurcation controller, and when a greater degree of uncertainty is apparent in the system or environment the

DAC method appears suitable.

ACKNOWLEDGEMENTS

This work was sponsored by the Science and Technology Facilities Council (STFC) and EADS Astrium UK Ltd through a CASE award (Blair Brown) and a European Research Council Advanced Investigator grant (VISIONSPACE 227571)(Colin McInnes).

REFERENCES

[1] Baoyin H. Gong S., Li J. Solar radition pressure used for formation flying around sun-earth libration point. *Applied Mathematics and Mechanics-English Edition*, 30:1009–1016, 2009.

[2] Scharf D.P., Ploen S.R., and Hadaegh F.Y. A survey of spacecraft formation flying guidance and control (part ii): Control. In *American Control Conference, Vol.4 p2976-2985*, Colorado, June 4-6, 2003,.

[3] Devaney R L Hirsch M W, Smale S. *Differential Equations, Dynamical Systems and An Introduction to Chaos*. Elsevier, 2004.

[4] Agiza H. El-Dessoky M. Global stabilization of some chaotic dynamical systems. *Chaos Solitions and Fractals*, 42:1584–1598, 2009.

[5] Holmes P Guckenheimer J. Structurally stable heteroclinic cycles. *Mathematical Proceeding to the Cambridge Philosophical Society*, 103:189–192, 1988.

[6] Li Z. Chaos induced by heteroclinic cycles connecting repellers and saddles in locally compact metic space. *Nonlinear Analysis-Theory Methods and Applications*, 71:1379–1388, 2009.

[7] Kuznetsov Y. *Elements of Applied Bifurcation Theory*. Springer, 2004.

[8] Celik C. Hopf bifurcation of a ratio-dependent predator-prey system with time delay. *Chaos Solitions and Fractals*, 42:1471–1484, 2009.

[9] Hutchinson S. Choset H., Lynch K. *Principles of Robot Motion*. Cambridge, 2005.

[10] Zeng J. Xue Z. Circle formation control of large-scale intelligent swarm systems in a distributed fashion. In *6th International Symposium on Neural Networks, Vol.5552 p1105-1115*, Wuhan, China, May 26-29, 2009,.

[11] Chellaboina V. Haddad W. *Nonlinear Dynamical Systems and Control: A Lyapunov-Based Approach*. Princeton University Press, 2008.

[12] Momeni H. Boroujeni E., Dadras S. An adaptive controller for a class of non-linear systems an application to ship roll motion. In *41st Southeastern Symposium on System Theory, p213-216*, Tullahoma TN, Mar 15-17, 2009,.

[13] Radice G. *Behavior Based Autonomy for Single and Multiple Spacecraft*. PhD thesis, University of Glasgow, 2002.

[14] Holmes P Guckenheimer J. Structurally stable heteroclinic cycles. *Mathematical Poceeding to the Cambridge Philosophical Society*, 103:189–192, 1988.

[15] Xie L. Chen H. A novel artificial potential field based reinforcement learning for mobile robitics in ambient intelligence. *International Journal of Robotics and Automation*, 24:245–254, 2009.

[16] Lugo-Gonzalez E. Ramirez-Gordillo J., Merchan-Cruz E. The laplacian artificial potential field for the path finding of robotic manipulators. In *5th Electronics, Robotics and Automative Mechanics Conference, p508-513*, Cuernavaca, Mexico, Sep 30-Oct 03, 2008,.

[17] Leger A. Cockell C., Herbst T. Darwin-an experimental astronomy mission to search for extrasolar planets. *Experimental Astronomy*, 23:435–461, 2009.

[18] Jennrich O. Lisa technology and instrumentation. *Classical and Quantum Gravity*, 26:153001, 2009.

[19] Bernstein D. S. Hong J. Adaptive stabilization of non-linear oscillators using direct adaptive control. *Internation Journal of Control*, 74:432–444, 2000.

[20] Bernstein D. S. Hong J., Cummings I. A. Experimental application of direct adaptive control laws for adaptive stabilization and command following. In *Conference on Decision and Control*, number TuM11-1440, Pheonix, December 1999.

[21] Houjun T. Yimei C., Zhengzhi H. Direct adaptive control for nonlinear uncertain system based on control lyapunov function method. *Journal of Systems Engineering and Electronics*, 17:619–623, 2006.

[22] McInnes C. R. Direct adaptive control for gravity-turn descent. *Journal of Guidance*, 22:374–377, 1998.